

Binding Studies of Cationic Conjugated Polymers and DNA for Label-Free Fluorescent Biosensors

*Pengbo Zhang,^{ab} Chang Lu,^b Chenqi Niu,^b Xiaoyu Wang,^c Zhengping Li,^{*a} Juewen Liu^{*b}*

^aSchool of Chemistry and Biological Engineering, University of Science and Technology
Beijing, 30 Xueyuan Road, Haidian District, Beijing, 100083, China

^bDepartment of Chemistry, Waterloo Institute for Nanotechnology, University of Waterloo, 200
University Avenue West, Waterloo, Ontario N2L 3G1, Canada.

^cSchool of Materials Science and Engineering, University of Science and Technology Beijing, 30
Xueyuan Road, Haidian District, Beijing, 100083, China

KEYWORDS: cationic conjugated polymers, DNA detection, biosensors, aptamers, fluorescence

ABSTRACT

Cationic conjugated polymers (CCPs), especially polythiophene, have been extensively used as probes for developing DNA and aptamer-based biosensors. Although many interesting applications have been achieved, fundamental understanding on this system remained quite limited. In this work, we performed systematic binding assays to understand the interactions between poly(3-(3'-N,N,N-triethylamino-1'-propyloxy)-4-methyl-2,5-thiophene (PMNT) and DNA. The fluorescence of PMNT at 530 nm initially decreased and then a peak at 580 nm emerged after binding with single-stranded DNA (ssDNA). The binding force between PMNT and DNA was dominated by electrostatic interactions at first and then DNA base-mediated interactions also became important. Since the bases in double-stranded DNA (dsDNA) were shielded, their fluorescence changes were quite different. To best differentiate ssDNA and dsDNA, the optimal pH was between 6 and 8, and the optimal NaCl concentration was around 0.3 M. Moreover, by changing the sequence and length of ssDNA, poly-T had the largest fluorescence shift and poly-A had the smallest change. Under the optimized condition, the PMNT-based biosensor had a detection limit of 1 nM DNA, which was similar to the SYBR Green I-based assay.

1. Introduction

Water-soluble cationic conjugated polymers (CCPs), such as poly(fluorene phenylene), polyfluorene and polythiophene, have been extensively used as optical probes for developing chemical and biological sensors due to their excellent light absorption and emission properties.¹⁻⁴ In particular, they have attracted much attention as probes for designing DNA and aptamer-based biosensors due to charge attraction.^{5,6} For example, Bazan and coworkers developed a fluorescence resonance energy transfer (FRET)-based DNA sensor using CCPs to sensitize the emission of fluorescein-tagged peptide nucleic acids (PNA). The CCP exhibited 25-fold higher fluorescence emission than those obtained by fluorescein only, resulting in the detection of 10 pM target DNA.⁷ By introducing ethidium bromide (EB), a duplex intercalator, the transition of DNA from a G-quadruplex to a duplex was monitored in real-time through FRET between CCPs, fluorescein and EB.⁸ Moreover, the Wang group utilized CCPs for the detection of genetic disorders, such as DNA methylation and single nucleotide polymorphism (SNP).⁹⁻¹² This strategy incorporated single base extension or polymerase chain reaction to generate large amounts of double-stranded DNA (dsDNA) labeled with fluorescein and detected the FRET signal generated from the complex of CCPs and dsDNA. These FRET-based sensors required the use of DNA intercalating dyes or covalent labeling of DNA.

Analyte-induced conformational change of CCPs allowed an alternative strategy to develop CCP-based biosensors, which do not require additional fluorophores on DNA. Leclerc and coworkers explored the optical properties associated with conformational change of polythiophenes when interacting with single-stranded DNA (ssDNA) and dsDNA.¹³ Polythiophenes were believed to form a highly conjugated and planar conformation when interacting with ssDNA and returned to a less conjugated conformation after complementary

DNA (cDNA) was added, which was deduced from the optical properties of the CCPs. This method was also applied to the detection of nucleases, nucleotide phosphates and ATP due to changes in the number of negative charges or hydrophobicity of targets.¹⁴⁻¹⁷ Due to conformational changes of aptamers after binding with targets, CCPs are useful for the fabrication of aptamer-based biosensors as well.¹⁸⁻²¹ For example, aptamers for potassium and α -thrombin can form G-quadruplex structures,¹⁷ while thymine-Hg²⁺-thymine interactions can fold DNA into duplex regions,^{22,23} both of which resulted in specific biosensors. The conformational change of CCPs was also used for the detection of bacteria.²⁴ In addition, CCPs, especially polythiophene, can be trapped and aligned into polyisocyanides to form a hybrid biomimetic hydrogel with a highly ordered conformation, which was used for anti-infection wound dressings.²⁵

While many interesting applications based on CCPs and DNA have been demonstrated, most of them only focused on improving the sensitivity and specificity for target detection, leaving fundamental understanding on this system largely unexplored. In this work, we aimed to perform systematic binding assays to understand the interactions between CCPs and DNA. Since electrostatic interactions are critical for their binding, we first varied the salt concentration and pH. In addition, we varied the sequence and length of DNA, which can also change the strength of charge attraction. Finally, we tested a label-free fluorescent CCP-based DNA biosensor under the optimized condition and compared it with SYBR Green I (SGI) staining.

2. Materials and Methods

2.1 Chemicals

The DNA samples used in this work were obtained from Integrated DNA Technologies (Coralville, IA, USA). The sequence of the ssDNA is 5'-CCC AGG TTC TCT TCA CAG ATG CGT-3', and its cDNA is 5'- ACG CAT CTG TGA AGA GAA CCT GGG-3'. Sodium chloride, sodium phosphate dibasic (Na₂HPO₄) and sodium phosphate monobasic anhydrous (NaH₂PO₄) were from Mandel Scientific (Guelph, ON, Canada). Poly(3-(3'-N,N,N-triethylamino-1'-propyloxy)-4-methyl-2,5-thiophene hydrochloride) (PMNT) was synthesized according to a previous report.²⁶ Milli-Q water was utilized for making all the buffers and solutions.

2.2 Fluorescence detection of PMNT

PMNT was excited at 392 nm and its emission was recorded from 450 nm to 650 nm. The fluorescence spectra of PMNT were recorded using a microplate reader (Tecan Spark). The dsDNA samples were prepared by incubating the ssDNA and its cDNA (100 μM each) at 95°C for 5 min and then slowly cooled to room temperature. Different concentrations of DNA were added into 10 mM phosphate buffer (PB), pH 7 with 0.3 M NaCl and 38 nM PMNT (based on the PMNT strand or 5 μM based on the monomer unit) to a final volume of 100 μL. After mixing, the fluorescence spectra and fluorescence polarization of PMNT were collected immediately. The peak intensities at 530 nm and 580 nm were used to calculate the fluorescence ratio. The dissociation constant (K_d) value was obtained based on the equation $F = F_{\max}X/(K_d + X) + F_0$. F represents the calculated fluorescence ratio of PMNT, F_{\max} stands for the maximum fluorescence ratio, X is the DNA concentration, and F_0 is the fluorescence ratio of the blank.

2.3 CCP-based label-free fluorescence assay

Different concentrations of cDNA were added into the mixture of 38 nM PMNT, 100 nM ssDNA in PB (pH 7) with 0.3 M NaCl. The fluorescence of PMNT was then detected and recorded.

2.4 SGI fluorescence assay

Different concentrations of cDNA were added into the mixture of 100 nM ssDNA and 0.5× SGI in PB (pH 7) with 0.3 M NaCl. SGI was excited at 470 nm and its emission was recorded from 515 nm to 620 nm.

2.5 Size distribution of the PMNT-DNA complexes

The hydrodynamic size of the PMNT-DNA complex was measured with a Malvern Zetasizer nano ZS instrument. 1 μM ssDNA or dsDNA was mixed with 38 nM PMNT in PB (pH 7) with 0.3 M NaCl to a final volume of 1 mL. After overnight incubation, the mixture was put into the cell and the measurement was performed at 25°C.

3. Results and Discussion

3.1 Effect of pH and salt concentration

The structure of PMNT is shown in Figure 1A. We chose PMNT as a model CCP since it showed an obvious conformational change when interacting with DNA.^{13, 26} Our PMNT has an average molecular weight of 38 kDa (polydispersity index 1.87), indicating that each PMNT chain contains on average 132 thiophene monomer units. While both the absorption and fluorescence of PMNT are sensitive to its conformation, fluorescence is more sensitive and thus we focused on its fluorescence. PMNT has a fluorescence emission peak at around 530 nm, which corresponds to a random-coiled nonplanar conformation. When interacting with a ssDNA, the 530 nm peak is quenched and a peak around 580 nm emerged due to the formation of a

highly conjugated, planar conformation. When complexed with a dsDNA, the fluorescence of PMNT at 530 nm is strongly quenched without showing the 580 nm peak.

Buffer environment may affect the interaction between CCPs and negatively charged DNA.^{27,28} To test this effect systematically, we first studied the effect of pH. A 24-mer ssDNA with a random sequence and its cDNA were used for this study. As shown in Figure 1 and Figure S1, pH had a huge influence, and the fluorescence difference between the ssDNA and dsDNA was the largest at close to neutral pH (pH 6 to 8).

When each pH was analyzed, the fluorescence of PMNT was greatly quenched after binding with the ssDNA, and an additional small peak appeared at 580 nm at pH 4 and 5, indicating a relatively weak binding between PMNT and ssDNA. At pH 6-8, the 580 nm peak increased sharply after adding the ssDNA, and the fluorescence at 530 nm showed a better recovery after interacting with the dsDNA. When the pH was further increased to 9, the phenomenon was similar to pH of 4 and 5. To quantitatively evaluate the influence of pH on fluorescence, we used the fluorescence ratio of 580 nm to 530 nm, which can minimize the variations caused by fluorescence intensity difference.

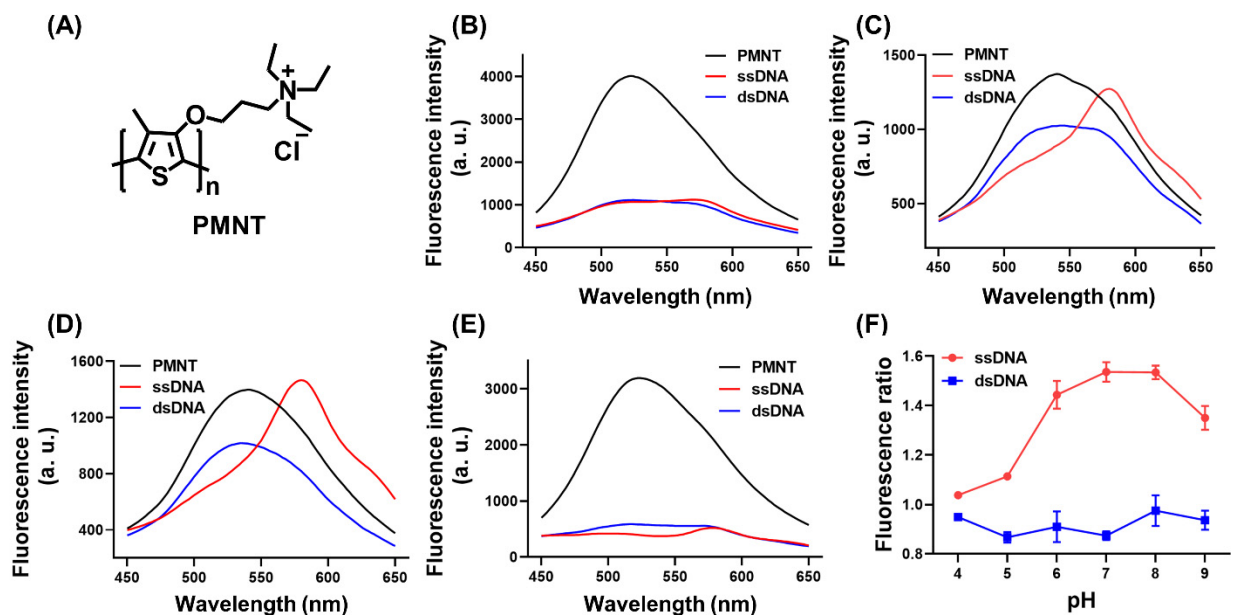


Figure 1. (A) The chemical structure of PMNT. The fluorescence spectra of PMNT (38 nM based on the strand of a single PMNT) after interacting with 100 nM ssDNA or dsDNA at (B) pH 4, (C) pH 6, (D) pH 7 and (E) pH 9. (F) The fluorescence ratio of PMNT at 580 nm to 530 nm in buffers with different pH values. The error bars are standard deviations from triplicate measurements.

Since the positive charges in PMNT were from a quaternary amine, the number of charges was not expected to change between pH 4 and 9. Therefore, the observed fluorescence difference was likely due to pH-dependent changes in the DNA. DNA bases are known to be (de)protonated beyond pH 4 and 9, which may destabilize duplex DNA. When interacting with a CCP, the destabilization effect might occur over an even broader pH range. From the analytical chemistry standpoint, the results in Figure 1F demonstrated that PMNT interacted better with ssDNA at pH 6-8, and we chose pH 7 as the optimal pH.

Since CCPs and DNA are believed to interact mainly via electrostatic interactions, we further assessed the effect of NaCl concentration at pH 7. With 0.1 M NaCl (Figure 2A), a small peak at 580 nm was observed for PMNT-ssDNA, and a relatively low fluorescence recovery at 530 nm was achieved for PMNT-dsDNA. When the concentration of NaCl was raised from 0.2 M to 0.4 M (Figure 2B-D), the change of the two peaks became more obvious. Finally, with 0.5 M NaCl (Figure 2E), the overall fluorescence drop with the DNA was quite small, regardless of ssDNA or dsDNA, indicating a strong charge screening effect, which weakened the interactions between PMNT and DNA.²⁹ These results illustrated that the optimal ionic strength was 0.3 M NaCl, and PMNT in PB (pH 7) with 0.3 M NaCl was initially in a random-coiled nonplanar conformation according to the 530 nm peak.

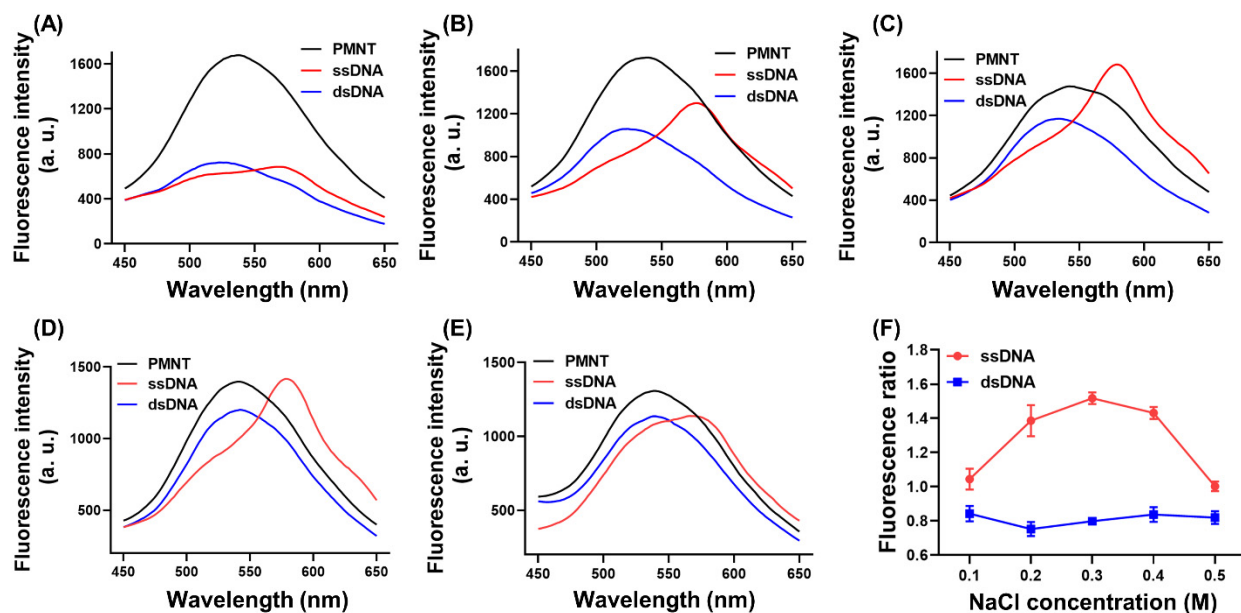


Figure 2. The fluorescence spectra of 38 nM PMNT (based on the PMNT strand) after interacting with 100 nM ssDNA or dsDNA at pH 7 with (A) 0.1 M, (B) 0.2 M, (C) 0.3 M, (D) 0.4 M and (E) 0.5 M NaCl. (F) The fluorescence ratio of PMNT at 580 nm to 530 nm in different NaCl concentrations.

3.2 Effect of DNA concentration

With a fixed PMNT concentration, the total positive-to-negative charge ratio would change when the concentration of DNA is changed. Understanding the effect of this ratio is critical for deciding an optimal probe DNA concentration. We then monitored the fluorescence intensity of PMNT by gradually increasing the concentration of ssDNA or dsDNA under the optimal buffer condition (0.3 M NaCl and pH 7). As shown in Figure 3A-3C, for the ssDNA, the maximum fluorescence at 530 nm was initially quenched at low ssDNA concentrations, whereas the 580 nm emerged at higher ssDNA concentrations. This observation was consistent with previous reports.^{13,23} The change of the fluorescence spectra was attributed to the association state of the PMNT-ssDNA complexes. At low DNA concentrations, the PMNT-ssDNA complex was likely overall positively charged as PMNT was in excess. When the DNA was in excess, the PMNT-ssDNA complex would be negatively charged. This difference might lead to different ways of packing PMNT around the DNA, resulting in different fluorescence properties. A strong 580 nm peak was indicative of better conjugation. By calculating the fluorescence ratio of 580 nm to 530 nm, a standard binding curve was plotted, and apparent K_d was calculated to be 55 nM (Figure 3D, red curve). It is worth noting that the maximum fluorescence ratio was achieved at about 200 nM DNA, where the total positive charges of 38 nM PMNT (equals to 5 μ M counting the monomer units) were comparable to the total negative charges of the ssDNA (23 negative charges for each 24-mer ssDNA). Once this ratio was reached, little further increase was observed in response to higher concentrations of ssDNA. While for the dsDNA, the fluorescence ratio was almost constant regardless of the dsDNA concentration (Figure 3D, blue squares). These results indicate that PMNT interacted with the ssDNA and dsDNA through different ways.

For detecting DNA, under our current conditions (38 nM PMNT), the probe DNA concentration should not exceed 200 nM.

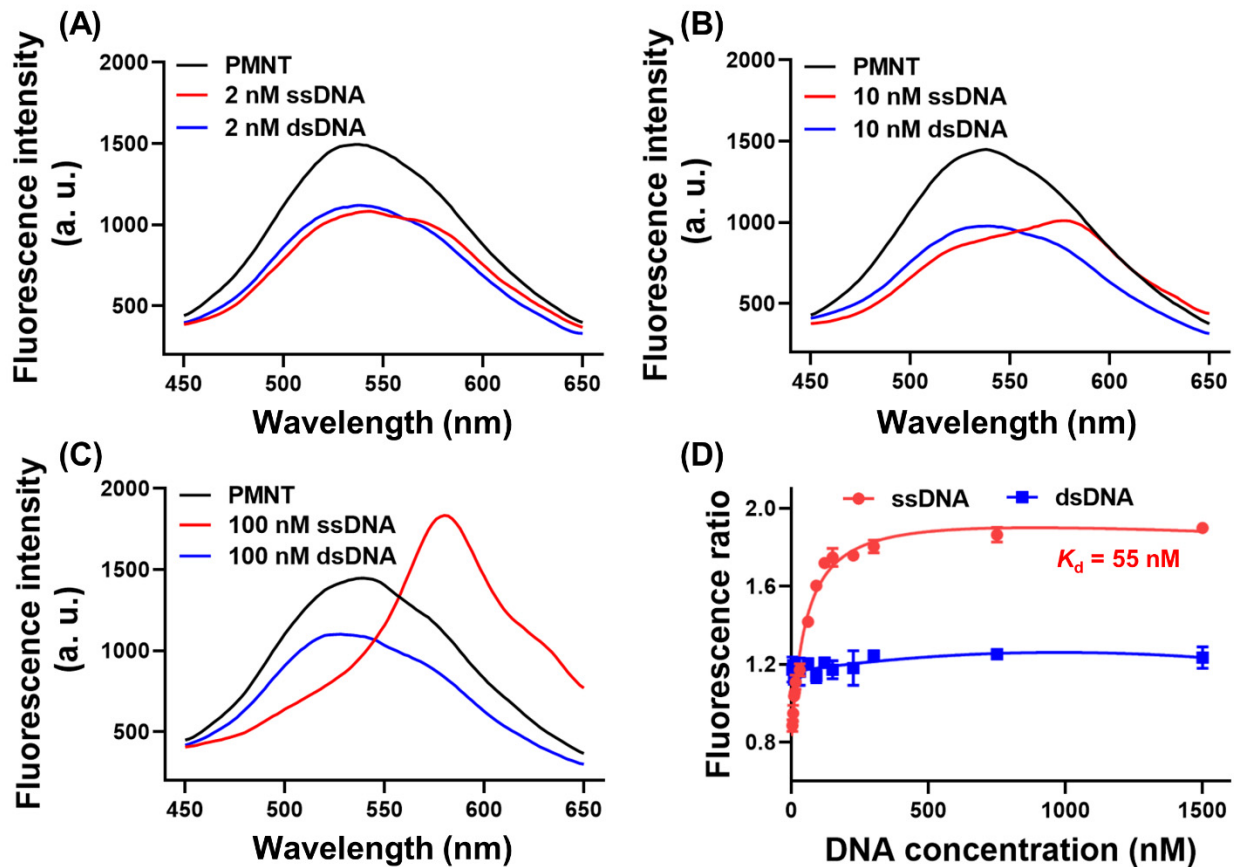


Figure 3. The fluorescence spectra of 38 nM PMNT after binding with ssDNA or dsDNA at DNA concentrations of (A) 2 nM, (B) 10 nM and (C) 100 nM. (D) The fluorescence ratio of PMNT at 580 nm to 530 nm in response to different concentrations of DNA. The error bars are standard deviations from triplicate measurements.

3.3 Binding mechanistic studies

To further understanding the binding mechanism between PMNT and DNA, we monitored the fluorescence polarization of PMNT-ssDNA and PMNT-dsDNA, respectively, which reflects the size of the binding complexes. As shown in Figure 4A, both PMNT-ssDNA and PMNT-dsDNA had an increase in polarization at lower DNA concentrations and then decreased with further increased DNA concentration. As dsDNA had more negative charges, the polarization changes of PMNT-dsDNA appeared earlier than the PMNT-ssDNA, demonstrating that the binding force between PMNT and DNA was primary electrostatic at the beginning. The relatively lower fluorescence polarization of PMNT-dsDNA at the final point indicated that PMNT formed a tighter structure by interacting with the dsDNA. The above measurements were performed in PB with 0.3 M NaCl. To test for generality, the same experiment was also repeated in 0.1 M NaCl to enhance electrostatic interactions (Figure S2), and the same trend was observed.

We further analyzed the size of the PMNT-DNA complexes using dynamic light scattering. As depicted in Figure 4B, PMNT-ssDNA formed dispersed aggregates with a diameter of about 175 nm in PB after overnight incubation, and PMNT-dsDNA formed aggregates of about 169 nm with a narrower size distribution concentrated in the smaller size region. This result was consistent with the fluorescence polarization data that the PMNT-dsDNA complex was smaller than the PMNT-ssDNA complex.

Considering the amphiphilic properties of both DNA (with hydrophobic bases and hydrophilic phosphate groups) and PMNT (with hydrophobic backbone and hydrophilic quaternary ammonium salt side chains), hydrophobic and π -stacking interactions between the hydrophobic PMNT backbone and DNA bases might also exist.³⁰ In a dsDNA, the DNA bases are shielded in the duplex structure and unavailable to interact with PMNT. Therefore, aside

from rigidity difference, the binding difference between ssDNA/dsDNA and PMNT might also exist due to DNA base related interactions.³¹

Based on the above results, a proposed binding mechanism between PMNT and ssDNA/dsDNA is depicted in Figure 4C. Free PMNT has a random-coil conformation. After adding a low concentration of DNA, where positive charges were in excess, the dominating electrostatic forces brought PMNT and DNA to proximity so that PMNT was stretched to a highly conjugated and planar conformation as mentioned above, which increased the size of the aggregates. At higher DNA concentrations, the electrostatic interactions between PMNT and DNA gradually saturated, and the interactions between the PMNT backbone and DNA bases become more important. For ssDNA, the interactions between the aromatic units of PMNT backbone and the exposed bases of ssDNA folded PMNT.³² The tight π -stacking between adjacent backbone of PMNT led to strongly red-shifted emission.^{33,34} While for the dsDNA, the bases are buried inside the duplex structure, which disfavored π -stacking interactions.³⁵ Thus, PMNT had to associate with the double helix of dsDNA to form more stable and compact aggregates. The extent of conjugation of PMNT was not changed significantly, resulting in merely decreased fluorescence of PMNT after binding with dsDNA.

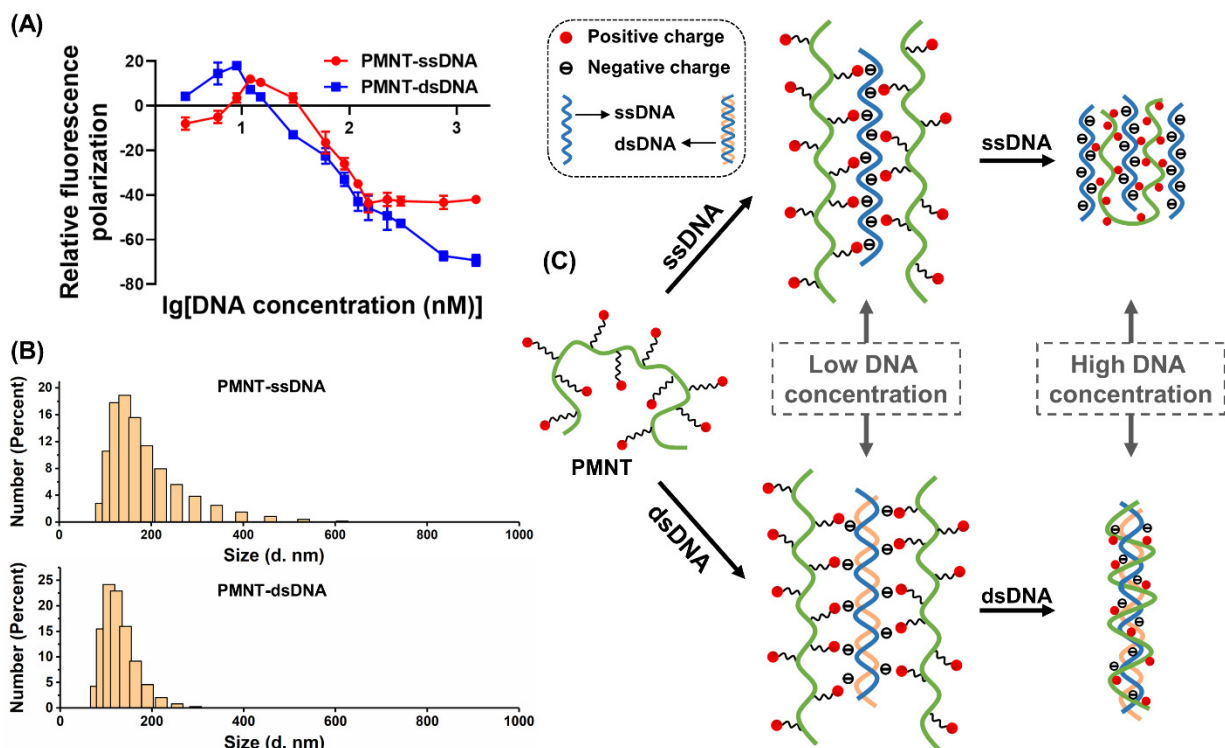


Figure 4. (A) The fluorescence polarization change of PMNT-ssDNA and PMNT-dsDNA complexes in response to different DNA concentrations. The error bars are standard deviations from triplicate measurements. (B) The hydrodynamic size distribution of PMNT-ssDNA and PMNT-dsDNA complex after overnight incubation. (C) A proposed scheme representing the binding mechanism between PMNT and ssDNA/dsDNA.

3.4 Effect of DNA length and sequence

Previous studies only focused on either random DNA or DNA aptamers, while a systematic understanding of DNA sequence and length is lacking. The sequence and length of ssDNA may cause different fluorescence responses of PMNT due to varied negative charge and base composition. Therefore, we then tested the influence of the DNA sequence on the fluorescence

of PMNT. As shown in Figure 5A, A30 DNA mainly decreased the fluorescence of PMNT at 530 nm, whereas T30, G18 and C30 all showed a peak at 580 nm. The complex of PMNT-T30 had the highest fluorescence at 580 nm, demonstrating that poly-T DNA can best stretch PMNT to form an optimal conjugated structure, which might be attributable to the weak intra-strand interactions in poly-T DNA.

To check the minimum length of ssDNA which can change the fluorescence of PMNT, the fluorescence spectra of PMNT after adding different lengths of poly-T were monitored (Figure 5B). T5 DNA only reduced the fluorescence of PMNT, and as short as T10 could induce the 580 nm peak and the effect saturated at T15. We further investigated the binding affinity between different DNA length and base by titrating DNA into a constant concentration of PMNT (Figure 5C and 5D). T30 showed a very high binding affinity, while the fluorescence of A30 and T5 was nearly unchanged with increasing DNA concentration. The apparent K_d was calculated to be 17 nM for 38 nM PMNT and 2 nM for 7.6 nM PMNT. Since the K_d changed with the PMNT concentration, the actual K_d was likely to be even lower than 2 nM,³⁶ demonstrating a very high binding affinity. A30 and T5 can also bind to PMNT, but such binding was not reflected from this fluorescence ratio (they can be observed from fluorescence intensity change). It is interesting to note that the fluorescence ratio of PMNT-T30 reached highest at 100 nM DNA for 38 nM PMNT and 40 nM for 7.6 nM PMNT. Considering the charge stoichiometry between PMNT and T30, a lower concentration of PMNT would show more accurate results.³⁶

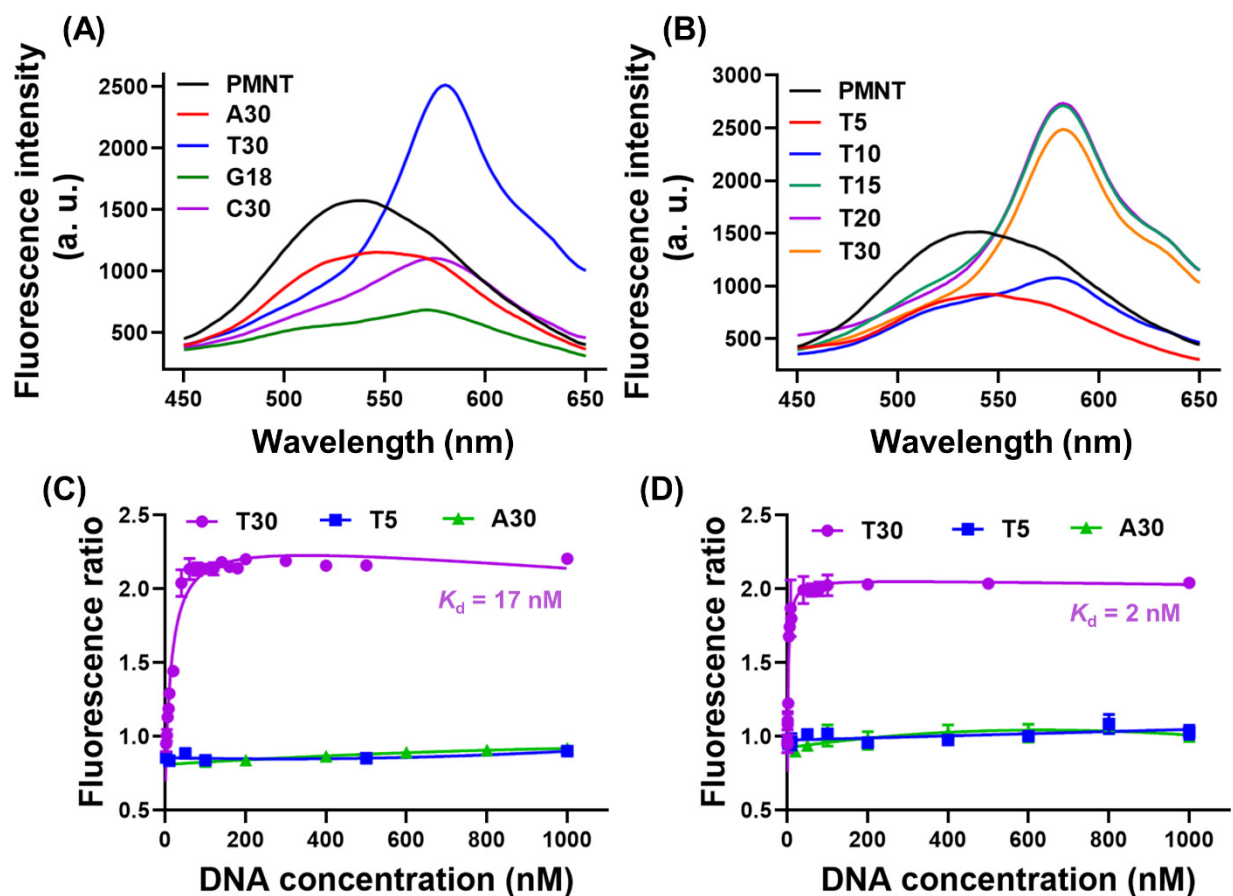


Figure 5. The fluorescence spectra of PMNT in the presence of ssDNA of (A) different sequences and (B) different lengths. The fluorescence ratio of 580 nm to 530 nm in response to different DNA concentrations with a constant PMNT concentration of (C) 38 nM and (D) 7.6 nM. The error bars are standard deviations from triplicate measurements.

3.5 DNA detection

Finally, we assessed the analytical performance of the CCP-based biosensor for DNA quantification by adding cDNA to the PMNT-ssDNA complex. As shown in Figure 6A, the fluorescence ratio decreased along with increased concentration of cDNA and as low as 1 nM

cDNA can be sensitively detected. The fluorescence ratio had a good linear range from 1 nM to 10 nM ($R^2 = 0.9295$) as shown in Figure S3A. The fluorescence of PMNT at 580 nm increased little after adding the same ssDNA as a non-complementary DNA control (Figure S4), demonstrating that our method has good specificity.

We further compared our results with another commonly used dye for label-free fluorescent DNA detection, SGI. As shown in Figure 6C and 6D, SGI obtained a similar result. The fluorescence signal of SGI has a good linear range from 1 nM to 10 nM ($R^2 = 0.9944$) as shown in Figure S3B. These results indicate that our CCP-based biosensor is as practical as SGI-based method. Although CCP and SGI have totally different mechanisms of binding to DNA, their similarity in analytical performance indicated that both methods can be analytically useful. Due to the potential health and environmental concerns of commercially DNA staining dyes, our CCP might be more biocompatible and more environmentally friendly.

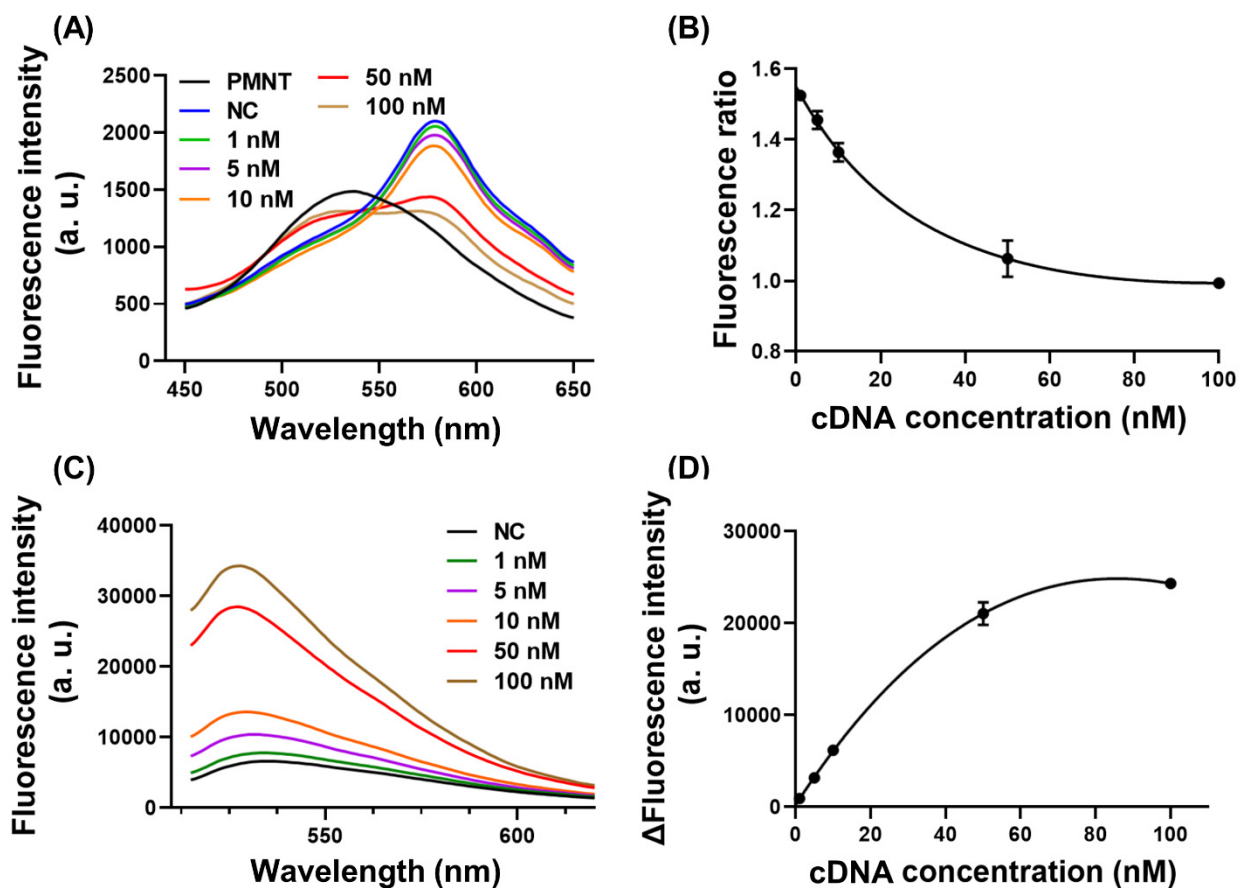


Figure 6. Evaluation of the CCP-based label-free biosensor for DNA detection. (A) The fluorescence spectra of (A) PMNT and (C) SGI by adding different concentrations of cDNA in the presence of 100 nM ssDNA. (B) The correlation between the fluorescence ratio of PMNT and the concentration of cDNA. (D) The correlation between the relative fluorescence intensity of $0.5\times$ SGI and the concentration of cDNA. The error bars are standard deviations from triplicate measurements.

4. Conclusions

In this work, we used PMNT as a model CCP to study the interactions between CCPs and DNA. Our results indicated that the binding force between PMNT and DNA was dominated by

electrostatic interactions between positively charged side chains of PMNT and negatively charged phosphates of DNA. In addition, interactions between the aromatic units of the PMNT backbone and the bases of DNA are also important. The different base exposure of ssDNA and dsDNA led to different binding modes with PMNT, resulting in ssDNA inducing a redshifted fluorescence and dsDNA only causing a decreased fluorescence of PMNT. The fluorescence polarization and dynamic light scattering results indicated that PMNT formed tighter complex by associating with the double helix of dsDNA with little conformational change compared with the random-coil conformation of free PMNT. From the results produced by ssDNA with different sequences and lengths, poly-T showed the highest fluorescence redshift while poly-A had the lowest shift, which might reflect the intra-strand interactions within DNA. The minimum length that can cause redshifted fluorescence of PMNT was 10. We further tested PMNT in a label-free fluorescent biosensor, and its performance was similar to that obtained from SGI-based assays.

ASSOCIATED CONTENT

The Supporting Information is available free of charge at <http://>

The fluorescence curve of PMNT after binding with ssDNA or dsDNA at pH 5 and 8 (Figure S1); the fluorescence polarization curve of PMNT-ssDNA and PMNT-dsDNA complex in response to different DNA concentrations in the buffer of 0.1 M NaCl (Figure S2) and the linear range of our CCP-based biosensor and SGI-based biosensor (Figure S3) (PDF)

AUTHOR INFORMATION

Corresponding Authors

Juewen Liu – Department of Chemistry, Waterloo Institute for Nanotechnology, University of Waterloo, Waterloo N2L 3G1 Ontario, Canada; orcid.org/0000-0001-5918-9336; Email: liujw@uwaterloo.ca

Zhengping Li - School of Chemistry and Biological Engineering, University of Science and Technology Beijing, Beijing, 100083, China; [orcid.org//0000-0002-7573-8822](https://orcid.org/0000-0002-7573-8822); Email: lzpbd@ustb.edu.cn

Authors

Pengbo Zhang - School of Chemistry and Biological Engineering, University of Science and Technology Beijing, Beijing, 100083, China; [orcid.org//0000-0002-8822-2868](https://orcid.org/0000-0002-8822-2868)

Chang Lu - Department of Chemistry, Waterloo Institute for Nanotechnology, University of Waterloo, Waterloo N2L 3G1 Ontario, Canada

Chenqi Niu - Department of Chemistry, Waterloo Institute for Nanotechnology, University of Waterloo, Waterloo N2L 3G1 Ontario, Canada

Xiaoyu Wang - School of Materials Science and Engineering, University of Science and Technology Beijing, Beijing, 100083, China

Author Contributions

The manuscript was written through contributions of all authors. All authors have given approval to the final version of the manuscript.

Notes

There are no conflicts to declare.

ACKNOWLEDGMENT

Funding for this work was from the Natural Sciences and Engineering Research Council of Canada (NSERC) and the Fundamental Research Funds for the Central Universities [FRF-IDRY-20-026 and FRF-BR-20-03B]. P. Zhang was supported by a China Scholarship Council (CSC) scholarship to visit the University of Waterloo.

REFERENCES

- (1) Feng, X.; Liu, L.; Wang, S.; Zhu, D. Water-soluble fluorescent conjugated polymers and their interactions with biomacromolecules for sensitive biosensors. *Chem. Soc. Rev.* **2010**, *39*, 2411-2419.
- (2) Wu, W.; Bazan, G. C.; Liu, B. Conjugated-polymer-amplified sensing, imaging, and therapy. *Chem* **2017**, *2*, 760-790.
- (3) Zhou, L.; Lv, F.; Liu, L.; Wang, S. Water-soluble conjugated organic molecules as optical and electrochemical materials for interdisciplinary biological applications. *Acc. Chem. Res.* **2019**, *52*, 3211-3222.
- (4) Xiao, F.; Fang, X.; Li, H.; Xue, H.; Wei, Z.; Zhang, W.; Zhu, Y.; Lin, L.; Zhao, Y.; Wu, C.; Tian, L. Light-Harvesting Fluorescent Spherical Nucleic Acids Self-Assembled from a DNA-Grafted Conjugated Polymer for Amplified Detection of Nucleic Acids. *Angew. Chem., Int. Ed.* **2022**, *61*, e202115812.
- (5) Zhu, C.; Liu, L.; Yang, Q.; Lv, F.; Wang, S. Water-soluble conjugated polymers for imaging, diagnosis, and therapy. *Chem. Rev.* **2012**, *112*, 4687-4735.

- (6) Lee, K.; Povlich, L. K.; Kim, J. Recent advances in fluorescent and colorimetric conjugated polymer-based biosensors. *Analyst* **2010**, *135*, 2179-2189.
- (7) Gaylord, B. S.; Heeger, A. J.; Bazan, G. C. DNA detection using water-soluble conjugated polymers and peptide nucleic acid probes. *Proc. Natl. Acad. Sc.* **2002**, *99*, 10954-10957.
- (8) He, F.; Tang, Y.; Yu, M.; Feng, F.; An, L.; Sun, H.; Wang, S.; Li, Y.; Zhu, D.; Bazan, G. C. Quadruplex-to-duplex transition of G-rich oligonucleotides probed by cationic water-soluble conjugated polyelectrolytes. *J. Am. Chem. Soc.* **2006**, *128*, 6764-6765.
- (9) Duan, X.; Liu, L.; Feng, F.; Wang, S. Cationic conjugated polymers for optical detection of DNA methylation, lesions, and single nucleotide polymorphisms. *Acc. Chem. Res.* **2010**, *43*, 260-270.
- (10) Feng, F.; Liu, L.; Wang, S. Fluorescent conjugated polymer-based FRET technique for detection of DNA methylation of cancer cells. *Nat. protoc.* **2010**, *5*, 1255-1264.
- (11) Duan, X.; Yue, W.; Liu, L.; Li, Z.; Li, Y.; He, F.; Zhu, D.; Zhou, G.; Wang, S. Single-nucleotide polymorphism (SNP) genotyping using cationic conjugated polymers in homogeneous solution. *Nat. Protoc.* **2009**, *4*, 984-991.
- (12) Zhang, P.; Qiu, T.; Liu, L.; Lv, F.; Li, Z.; Ying, J.; Wang, S. Conjoint analysis of DNA methylation for tumor differentiation using cationic conjugated polymers. *ACS Appl. Bio Mater.* **2020**, *3*, 2867-2872.

- (13) Ho, H. A.; Boissinot, M.; Bergeron, M. G.; Corbeil, G.; Doré, K.; Boudreau, D.; Leclerc, M. Colorimetric and fluorometric detection of nucleic acids using cationic polythiophene derivatives. *Angew. Chem., Int. Ed.* **2002**, *114*, 1618-1621.
- (14) Zhang, Y.; Li, Z.; Cheng, Y.; Lv, X. Colorimetric detection of microRNA and RNase H activity in homogeneous solution with cationic polythiophene derivative. *Chem. Commun.* **2009**, *22*, 3172-3174.
- (15) Yao, Z.; Feng, X.; Hong, W.; Li, C.; Shi, G. A simple approach for the discrimination of nucleotides based on a water-soluble polythiophene derivative. *Chem. Commun.* **2009**, *31*, 4696-4698.
- (16) Li, C.; Numata, M.; Takeuchi, M.; Shinkai, S. A sensitive colorimetric and fluorescent probe based on a polythiophene derivative for the detection of ATP. *Angew. Chem., Int. Ed.* **2005**, *117*, 6529-6532.
- (17) Ho, H. A.; Leclerc, M. Optical sensors based on hybrid aptamer/conjugated polymer complexes. *J. Am. Chem. Soc.* **2004**, *126*, 1384-1387.
- (18) Sinsinbar, G.; Palaniappan, A.; Yildiz, U. H.; Liedberg, B. A Perspective on Polythiophenes as Conformation Dependent Optical Reporters for Label-Free Bioanalytics. *ACS Sens.* **2022**, *7*, 686-703.
- (19) Liu, M.; Li, J.; Li, B. A colorimetric aptamer biosensor based on cationic polythiophene derivative as peroxidase mimetics for the ultrasensitive detection of thrombin. *Talanta* **2017**, *175*, 224-228.

- (20) Béra Abérem, M.; Najari, A.; Ho, H. A.; Gravel, J. F.; Nobert, P.; Boudreau, D.; Leclerc, M. Protein Detecting Arrays Based on Cationic Polythiophene–DNA–Aptamer Complexes. *Adv. Mater.* **2006**, *18*, 2703-2707.
- (21) Huang, B.; Geng, Z.; Yan, S.; Li, Z.; Cai, J.; Wang, Z. Water-soluble conjugated polymer as a fluorescent probe for monitoring adenosine triphosphate level fluctuation in cell membranes during cell apoptosis and in vivo. *Anal. Chem.* **2017**, *89*, 8816-8821.
- (22) Tang, Y.; He, F.; Yu, M.; Feng, F.; An, L.; Sun, H.; Wang, S.; Li, Y.; Zhu, D. A reversible and highly selective fluorescent sensor for mercury (II) using poly(thiophene)s that contain thymine moieties. *Macromol. Rapid Commun.* **2006**, *27*, 389-392.
- (23) Liu, X.; Tang, Y.; Wang, L.; Zhang, J.; Song, S.; Fan, C.; Wang, S. Optical detection of mercury (II) in aqueous solutions by using conjugated polymers and label-free oligonucleotides. *Adv. Mater.* **2007**, *19*, 1471-1474.
- (24) Sinsinbar, G.; Palaniappan, A.; Yildiz, U. H.; Liedberg, B. A Perspective on Polythiophenes as Conformation Dependent Optical Reporters for Label-Free Bioanalytics. *ACS Sen.* **2022**, *7*, 686-703.
- (25) Yuan, H.; Zhan, Y.; Rowan, A. E.; Xing, C.; Kouwer, P. H. Biomimetic networks with enhanced photodynamic antimicrobial activity from conjugated polythiophene/polyisocyanide hybrid hydrogels. *Angew. Chem., Int. Ed.* **2020**, *59*, 2720-2724.
- (26) Tang, Y.; Feng, F.; He, F.; Wang, S.; Li, Y.; Zhu, D. Direct visualization of enzymatic cleavage and oxidative damage by hydroxyl radicals of single-stranded DNA with a cationic polythiophene derivative. *J. Am. Chem. Soc.* **2006**, *128*, 14972-14976.

- (27) Ho, H. A.; Leclerc, M. New colorimetric and fluorometric chemosensor based on a cationic polythiophene derivative for iodide-specific detection. *J. Am. Chem. Soc.* **2003**, *125*, 4412-4413.
- (28) Wang, L.; Liu, X.; Yang, Q.; Fan, Q.; Song, S.; Fan, C.; Huang, W. A colorimetric strategy based on a water-soluble conjugated polymer for sensing pH-driven conformational conversion of DNA i-motif structure. *Biosens. Bioelectron.* **2010**, *25*, 1838-1842.
- (29) Taira, S.; Yokoyama, K. Self-assembly DNA-conjugated polymer for detection of single nucleotide polymorphism. *Biotechnol. Bioeng.* **2004**, *88*, 35-41.
- (30) Xia, F.; Zuo, X.; Yang, R.; Xiao, Y.; Kang, D.; Vallée-Bélisle, A.; Gong, X.; Heeger, A. J.; Plaxco, K. W. On the binding of cationic, water-soluble conjugated polymers to DNA: electrostatic and hydrophobic interactions. *J. Am. Chem. Soc.* **2010**, *132*, 1252-1254.
- (31) Huang, Y.; Liu, X.; Fan, Q.; Wang, L.; Song, S.; Wang, L.; Fan, C.; Huang, W. Tuning backbones and side-chains of cationic conjugated polymers for optical signal amplification of fluorescent DNA detection. *Biosens. Bioelectron.* **2009**, *24*, 2973-2978.
- (32) Liu, B.; Gaylord, B. S.; Wang, S.; Bazan, G. C. Effect of chromophore-charge distance on the energy transfer properties of water-soluble conjugated oligomers. *J. Am. Chem. Soc.* **2003**, *125*, 6705-6714.
- (33) Pinto, M. R.; Kristal, B. M.; Schanze, K. S. A water-soluble poly (phenylene ethynylene) with pendant phosphonate groups. Synthesis, photophysics, and layer-by-layer self-assembled films. *Langmuir* **2003**, *19*, 6523-6533.

- (34) Tan, C.; Pinto, M. R.; Schanze, K. S. Photophysics, aggregation and amplified quenching of a water-soluble poly (phenylene ethynylene). *Chem. Commun.* **2002**, *5*, 446-447.
- (35) Diogo, M. M.; Queiroz, J. A.; Monteiro, G. A.; Martins, S. A. M.; Ferreira, G. N. M.; Prazeres, D. M. F. Purification of a cystic fibrosis plasmid vector for gene therapy using hydrophobic interaction chromatography. *Biotechnol. Bioeng.* **2000**, *68*, 576-583.
- (36) Jarmoskaite, I.; AlSadhan, I.; Vaidyanathan, P. P.; Herschlag, D. How to measure and evaluate binding affinities. *eLife* **2020**, *9*, e57264.

Table of Contents

